journal of the mechanical behavior of biomedical materials 142 (2023) 105799

Contents lists available at ScienceDirect

Journal of the Mechanical Behavior of Biomedical Materials

journal homepage: www.elsevier.com/locate/jmbbm

Effect of 3D printing system and post-curing atmosphere on micro- and nano-wear of additive-manufactured occlusal splint materials

Junichiro Wada [a,b,*], Kanae Wada [a,c], Sufyan Garoushi [a], Akikazu Shinya [a,d], Noriyuki Wakabayashi [b], Tsutomu Iwamoto [c], Pekka K. Vallittu [a,e], Lippo Lassila [a]

[a] Department of Biomaterials Science, Turku Clinical Biomaterials Centre - TCBC, Institute of Dentistry, University of Turku, Itäinen Pitkäkatu 4B, Turku, 20520, Finland
[b] Department of Advanced Prosthodontics, Tokyo Medical and Dental University - TMDU, 1-5-45, Yushima, Bunkyo-ku, Tokyo, 113-8510, Japan
[c] Department of Pediatric Dentistry / Special Needs Dentistry, Tokyo Medical and Dental University – TMDU, 1-5-45, Yushima, Bunkyo-ku, Tokyo, 113-8510, Japan
[d] Department of Dental Materials Sciences, School of Life Dentistry at Tokyo, The Nippon Dental University, Japan
[e] Wellbeing Services County of South-West Finland, Lemminkäisenkatu 23, 20520, Turku, Finland

ARTICLE INFO

Keywords:
Additive manufacturing
CAD/CAM
Nitrogen gas
Occlusal splint
Post-curing
Two-body wear

ABSTRACT

Although additive manufacturing has been widely applied for occlusal splint (OS) fabrication, it is still unclear whether 3D printing system and post-curing atmosphere would play a role in the wear resistance of additive-manufactured OS. Therefore, the aim of this study was to evaluate the effect of 3D printing system (liquid crystal display (LCD) and digital light processing (DLP)) and post-curing atmosphere (air and nitrogen gas (N_2)) on the wear resistance of hard and soft OS materials for additive-manufactured OSs (KeySplint® Hard and Soft). The evaluated properties were microwear (by two-body wear test) and nano-wear resistances (by nano-indentation wear test) as well as flexural strength and flexural modulus (by three-point bending test), surface microhardness (by Vickers hardness test), and nanoscale elastic modulus (reduced elastic modulus) and nano surface hardness (by nanoindentation test). For the hard material, the surface microhardness, microwear resistance, reduced elastic modulus, nano surface hardness, and nano-wear resistance were significantly affected by the printing system ($p < 0.05$), while all the evaluated properties except flexural modulus were significantly affected by the post-curing atmosphere ($p < 0.05$). Meanwhile, both the printing system and post-curing atmosphere significantly affected all the evaluated properties ($p < 0.05$). The specimens additive-manufactured by DLP printer tended to show higher wear resistance in the hard material groups and lower wear resistance in the soft material groups when compared to those by LCD printer. The post-curing at N_2 atmosphere significantly enhanced the microwear resistance of hard material groups additive-manufactured by the DLP printer ($p < 0.05$) and soft material groups additive-manufactured by the LCD printer ($p < 0.01$), while it significantly enhanced the nano-wear resistance of both hard and soft material groups regardless of the printing system ($p < 0.01$). It can be concluded that 3D printing system and post-curing atmosphere affect the micro- and nano-wear resistance of tested additively manufactured OS materials. In addition, it can be also concluded that the optical printing system providing higher wear resistance depends on the material type, and using nitrogen gas as a protection gas during post-curing enhances the wear resistance of tested materials.

1. Introduction

An occlusal splint (OS) is a common oral appliance for the treatment of temporomandibular joint disorder (TMD) (Klasser and Greene, 2009; Al-Moraissi et al., 2020), the protection of fixed prostheses from fractures due to unexpected occlusal stress (Beier et al., 2012), and long-term survival of periodontally weakened teeth (McGuire and Nunn, 1996). Patients generally wear OSs during sleeping and OSs are exposed to occlusal stress including, tapping, clenching, and grinding (Sjöholm, 1995; Tokiwa et al., 2008). To achieve desired outcomes of TMD

Abbreviations: AFM, atomic force microscopy; DLP, digital light processing; LCD, liquid crystal display; N_2, nitrogen gas; OS, occlusal splint; PMMA, polymethylmethacrylate; TMD, temporomandibular joint disorder; VHN, Vickers hardness number.

* Corresponding author. Department of Advanced Prosthodontics, Tokyo Medical and Dental University - TMDU, 1-5-45, Yushima, Bunkyo-ku, Tokyo, 113-8510, Japan.
E-mail address: wadajun.rpro@tmd.ac.jp (J. Wada).

https://doi.org/10.1016/j.jmbbm.2023.105799
Received 18 January 2023; Received in revised form 10 March 2023; Accepted 23 March 2023
Available online 24 March 2023

treatment or the long-term maintenance of remaining teeth and/or fixed prostheses, OSs are occasionally long-term used (Sjoholm et al., 2014; Faus-Matoses et al., 2020).

OSs can be classified into two types such as hard and soft types based on their physical properties. Several previous studies have indicated that hard OSs with high surface hardness would show better clinical performance than soft OSs from the viewpoint of therapeutic effectiveness (Okeson, 1987; Cruz-Reyes et al., 2011). On the other hand, a few studies have suggested that soft OSs would be more effective than hard OSs from the viewpoint of stress on the antagonist (Halachmi et al., 2008) and patient comfortableness (Ariji et al., 2016; Sriharsha et al., 2018). Therefore, although hard materials are more common for OS fabrication, both hard and soft materials are clinically needed. Additionally, clinicians should understand the physical properties of each material and select appropriate material for OS based on the treatment purpose and/or individual patient's preference.

Recently, digital technology has been widely applied to the dental field. Digital procedures to fabricate dental objects can be mainly classified as either milling or additive manufacturing (Tigmeanu et al., 2022; Anadioti et al., 2022). Milling can provide dental objects with homogeneity, solidity, and well-fitness (Ellakany et al., 2022; Al Hamad et al., 2022), indicating it would be suitable for the fabrication of definitive dental prostheses, such as fixed crowns and bridges. Meanwhile, additive manufacturing can provide them with minimal material waste and low cost (Goodacre and Goodacre, 2022), indicating it would be suitable for the fabrication of surgical guides, custom trays, and OSs. There are several materials used for OS fabrication with various chemical compositions available for additive manufacturing. A previous study reported that those materials for additive-manufactured OSs generally showed lower wear resistance than heat-cured or milled polymethylmethacrylate (PMMA) regardless of their chemical compositions (Grymak et al., 2022). On the other hand, the stereolithography printing system is commonly used for OS fabrication in additive manufacturing systems, and 3D printers can be mainly classified into two types based on liquid crystal display (LCD) and digital light processing (DLP) as the principles of pattern formation (Quan et al., 2020). DLP printers can produce objects more effectively due to their higher light intensity (Revilla-León and Özcan, 2019), while it has been reported that LCD printers would produce objects with a smoother surface, especially in OS fabrication (Wada et al., 2022a, 2022b). Additionally, as well as the printing system, post-curing methods can affect the physical properties of additive-manufactured objects (Kunjan et al., 2006; Al Mortadi et al., 2012). Using a nitrogen gas (N_2) as a post-curing atmosphere has been reported to be effective to prevent oxygen-inhibited layer formation and enhance the physical properties of additive-manufactured objects (Wada et al., 2022a, 2022b; Reymus et al., 2019). Although several studies have evaluated the wear resistance of OS materials (Kurt et al., 2012; Lutz et al., 2019; Gibreel et al., 2022), the effect of the printing system and post-curing method on the wear resistance of additive-manufactured OSs is still unclear.

Therefore, the aim of this study was to evaluate the effect of 3D printing system (LCD and DLP printers) and post-curing atmosphere (the air and N_2 atmospheres) on the wear resistance of additive-manufactured hard and soft OS materials based on methacrylate. The evaluated properties were micro- and nano-wear resistances as well as flexural strength, flexural modulus, microhardness, reduced elastic modulus, and nano surface hardness. The null hypotheses were as follows: (1) the 3D printing system would not affect the wear resistance of evaluated additive-manufactured OS materials, and (2) the post-curing atmosphere would not affect their wear resistance.

2. Materials and methods

2.1. Tested materials

Two different materials for additive-manufactured OS were tested in this study. One was material for hard OS (KeySplint® Hard, Keystone Industries GmbH, Singen, Germany) and another was material for soft OS (KeySplint® Soft, Keystone Industries GmbH, Singen, Germany). Both materials were photopolymerizing polymers based on methacrylate, photo-initiator, inhibitor, and pigment. It was noted that detailed information about materials composition was not available from Manufacturer.

2.2. Specimen fabrication

According to the previous study (Wada et al., 2023), 80 bar-shaped specimens (3.5 mm × 10.0 mm × 60.0 mm) were fabricated in this study (Fig. 1). Half of the specimens (n = 40) were made of KeySplint® Hard as hard specimens, while the other half (n = 40) were made of KeySplint® Soft as soft specimens. For the fabrication of both hard and soft specimens, half of them (n = 20) were additive-manufactured using an LCD printer of which the LED wavelength was 405 nm (Creo™ C5, PLANMECA OY, Helsinki, Finland) (Creo group), while the other half (n = 20) were printed by a digital light processing (DLP) printer with 385 nm (Asiga MAX™, SCHEU-DENTAL GmbH, Iserlohn, Germany) (Asiga group). Each additive manufacturing was performed with a print orientation of 90° and a layer thickness of 100 μm (Fig. 2). After additive manufacturing, each specimen was rinsed with isopropanol for 10 min in an ultrasonic cleaning unit (Quantrex® 90, L&R Ultrasonics, Kearny, NJ, USA), followed by stroboscopic post-curing with 2000 flashes on each surface (Otoflash G171, BEGO GmbH & Co, Bremen, Germany) in the following two different atmospheres: half of the specimens (n = 10/subgroup) were post-cured in the air with an absence of N_2 atmosphere (without N_2), while the other half (n = 10/subgroup) were post-cured at an N_2 atmosphere (with N_2). Both surfaces of each post-cured specimen were polished with wet polishing using a silicon carbide grinding paper 4000-grit with a grain size of 5 μm (SiC Paper #4000, Struers LLC, Cleveland, USA). The size of each polished specimen was standardized with a dimension of 3.0 mm (height) × 10.0 mm (width) × 60.0 mm (length), representing that the surface layers with around 250 μm thickness were removed from the as-manufactured specimens for being polished up.

2.3. Flexural strength, flexural modulus, and broken ratio

To assess the flexural strength and flextural modulus, a three-point bending test was performed for each specimen by a universal testing machine (Model LRX; Lloyds Instruments Ltd, Hampshire, UK). The test was performed with the crosshead speed of 5.0 mm/min and the span length of 50 mm in the air atmosphere at 23.0 ± 1 °C using a load cell with a capacity of 2500 N. Each test was detected to be finished based on one of the following test conditions: 1) the load reduction reached 10% of the maximum load; 2) the specimen deflection reached 12 mm, or 3) the specimen was broken. Flexural strength (σ) was calculated in MPa using the following equation:

$$\sigma = \frac{3FL}{2b \times h^2}$$

where F is the maximum load applied to the specimen (N), L is the span length (50 mm), b and h are the width (10 mm) and height (3 mm) of specimen, respectively. Meanwhile, flexural modulus (E) was calculated in MPa using the following equation:

$$E = \frac{F}{d} \times \frac{L^3}{4b \times h^3}$$

where F/d is the gradient of load versus deflection curve at the linear section, L is the span length (50 mm), b and h are the width (10 mm) and height (3 mm) of specimen, respectively. In this study, flexural modulus was conveniently converted from MPa to GPa.

Additionally, for each group, the ratio of number of broken

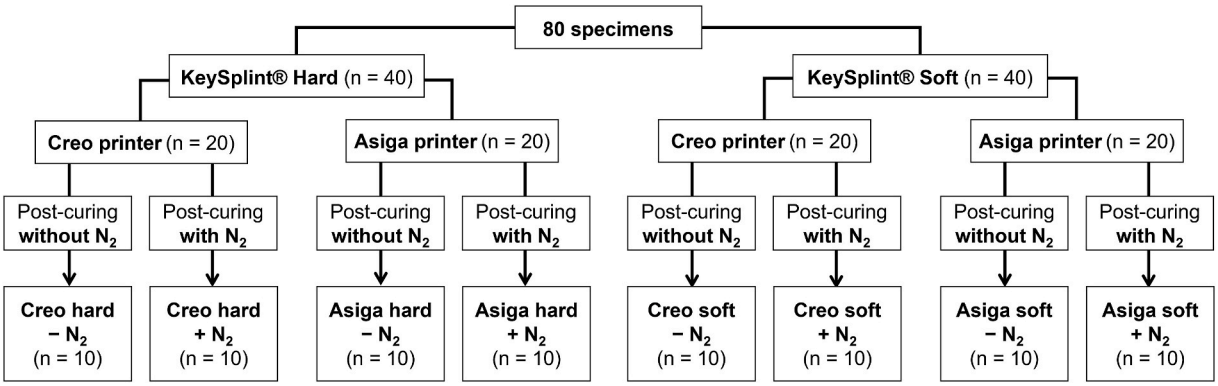

Fig. 1. Flowchart of specimen fabrication. Post-curing without N_2: stroboscopic post-curing in the air atmosphere. Post-curing with N_2: stroboscopic post-curing at a nitrogen gas atmosphere.

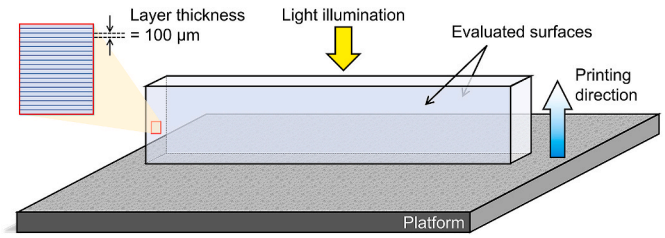

Fig. 2. The printing direction (gradated blue arrow), direction of light illumination (yellow arrows), and evaluated surfaces.

specimens to total number (n = 10) was calculated as the broken ratio (%).

2.4. Microhardness (Vickers hardness)

For each subgroup, two specimens were randomly selected for microhardness measurements. Using a Vickers hardness testing device (Duramin-5, Struers, Ballerup, Denmark), the square-based pyramid indentations were impressed on 10 different regions on each selected specimen. The indenting force was 9.81 N and the application time was 5 s. The diagonals of impressed indentation were measured, and Vickers hardness number (VHN) was calculated as the microhardness using the following equation:

$$VHN = \frac{0.1891 \times F}{d^2}$$

where F is the indenting force (N) (9.81 N), and d is the mean length of the diagonals of impressed indentation (mm).

2.5. Microwear resistance (microwear depth)

Six specimens were randomly selected from each group and sectioned for the microwear test (3.0 mm × 10.0 mm × 15.0 mm). In this study, the two-body wear test was performed as a microwear test according to the previous studies (Garoushi et al., 2021; Oja et al., 2021; Gibreel et al., 2022) to demonstrate the wear characteristics of OS materials during sleep without any food. All sectioned specimens were stored in water at 37.0 °C for 24 h before testing. The microwear test was performed using a chewing simulator (CS-4.2, SD Mechatronik, Feldkirchen- Westerham, Germany) which consisted of two different chambers simulating vertical and horizontal movements sequentially in the presence of water. Each chamber includes a lower sample holder to insert the specimen and an upper loading tip as the antagonist of tested specimens. A steatite ball with a diameter of 6 mm was used as the upper antagonist. For each selected specimen, 15000 simulation chewing cycles were performed at 1.5 Hz with a vertical weight of 2 kg, simulating a chewing force of 20 N. Wear patterns were scanned using a 3D optical profilometer (OP) (ContourGT-I, Bruker Nano, Inc., Tucson, AZ, USA), and the average of deepest points of 6 profiles scanned in each specimen was calculated as microwear depth (μm), which was the representative value of microwear resistance.

2.6. Nanoindentation (reduced elastic modulus and nano surface hardness)

One specimen was randomly selected from each group for the nanoindentation test. Using a nanoindentation device (TI-750 ubi, Hysitron, Minneapolis, MN, USA) with the cube corner indenter with a face angle of 35.26 °with respect to the indentation vertical axis, the nanoindentation test was performed at 23.0 ± 1 °C according to Oliver and Pharr method (Oliver and Pharr, 2004). The indenting load and displacement resolution of the device were 1.0 mN and 0.1 nm, respectively. The indentations were impressed on 5 different regions on each selected specimen (n = 5). The indentation load was up to a maximum force of 1000 mN with a constant indenting speed of 200 mN/s. After the indentation, the load-displacement curve was generated, and reduced elastic modulus (E) and nano surface hardness (H) were calculated using a software (TriboScan, version 9.1.1.0, Hysitron, Minneapolis, MN, USA).

The reduced elastic modulus was calculated based on the slope of the upper portion of the unloading curve in the load-displacement curve. It has been reported that the modulus acquired from the load-displacement curve incorporated the stiffness of the specimen and the indenter and was previously defined as the reduced elastic modulus (Willems et al., 1993; Li et al., 2005). The relationship between the reduced elastic modulus and elastic modulus of a material is given by the following equation:

$$\frac{1}{E^*} = \frac{1 - v_m^2}{E_m} + \frac{1 - v_i^2}{E_i}$$

where E* is the reduced elastic modulus (GPa); v_m is Poisson's ratio of the material; E_m is the elastic modulus of the material (GPa); v_i is the Poisson's ratio of the indenter, and E_i is the elastic modulus of the indenter. The v_i and E_i for the diamond indenter used in this study were 0.07 and 1141 GPa, respectively (Li and Bhushan, 2002), indicating that $(1 - v_i^2)/E_i$ could be assumed as 0. The mean reduced elastic modulus of 5 indentations was calculated as the representative data. Meanwhile, nano surface hardness (residual hardness) was acquired based on the depth-sensing indentation instruments according to the following equation:

$$NH = \frac{P}{A_i}$$

where NH is nano surface hardness (MPa); P is the applied load (N) and A_i is the projected area of indentation. The mean value of 5 indentations was calculated as the representative data of nano surface hardness.

Additionally, a nanoindentation test was performed for conventional heat-cured (Paladon 65, Kulzer GmbH, Hanau, Germany) and autopolymerizing (Palapress, Kulzer GmbH, Hanau, Germany) resins in the same manner for additive-manufactured OS materials because of a lack of information referring their nanoscale physical properties in previous studies. The specimens were fabricated in accordance with the manufacturer's instructions, as stated in previous studies (3.0 mm × 10.0 mm × 15.0 mm) (Gibreel et al., 2021; Perea-Lowery et al., 2021).

2.7. Nano-wear resistance (nano-wear depth)

Using the nanoindentation device (TI-750 ubi) with the three-sided pyramidal indentation same as in 2.5., a nanoscale wear test was performed for additive-manufactured OS materials as well as conventional heat-cured and autopolymerizing resins. The wearing rate was constant at 30 μm/s and the wearing force was 3–10 mN according to the previous study (Hamanaka et al., 2016). A wearing area created with 25 wearing cycles was 10 mm × 10 mm. The deepest depth of the wearing area was recorded as the nano-wear depth and analyzed using the software (TriboScan). The deepest wear depth was measured in 5 different cross-sections for each wearing area, and the average of the depth in 5 cross-sections was calculated as the nano-wear depth (μm), which was the representative value of nano-wear resistance. All testing was performed under uniform atmospheric conditions with a temperature of 23.0 ± 1 °C and humidity of 50 ± 1%. Additionally, an atomic force microscopy (AFM) image of each specimen after the nanoscale wear test was visually inspected using the nanoindentation device (TI-750 ubi) with a scan rate of 0.50 Hz, a tip velocity of 30.0 μm/s, a scan size of 30.0 μm, and a contacting force of 2.0 μN.

2.8. Statistical analysis

The statistical analysis was performed for each material (hard and soft) separately. Two predictors including the printing system and post-curing atmosphere were tested for all the evaluated data except the broken ratio using a 2-way analysis of variance (ANOVA). For each material, a 1-way ANOVA and Tukey's multiple comparisons as a post hoc analysis were performed among 4 subgroups (Fig. 1) for the flexural strength, flexural modulus, microhardness, and microwear resistance, while they were performed among 4 subgroups and 2 conventional resins (heat-cured resin and autopolymerizing resin) for the nano surface hardness, reduced elastic modulus, and nano-wear resistance. Regarding the broken ratio of specimens during a three-point bending test, the Chi-squared test was performed for the comparison between specimens post-cured without and with N_2 independently within each subgroup classified based on the material and printing system. A statistical software (IBM SPSS Statistics v28.0, IBM, Redmond, WA, USA) was used for all the statical analyses with the significance level set at 0.05.

3. Results

For the hard material, 2-way ANOVA revealed that the printing system significantly affected the microhardness ($p < 0.001$), microwear resistance ($p = 0.013$), nano surface hardness ($p < 0.001$), reduced elastic modulus ($p < 0.001$), and nano-wear resistance ($p < 0.001$), while the post-curing atmosphere significantly affected the flexural strength ($p = 0.002$), microhardness ($p < 0.001$), microwear resistance ($p = 0.021$), nano surface hardness ($p < 0.001$), reduced elastic modulus ($p < 0.001$), and nano-wear resistance ($p < 0.001$). Especially for nano-wear resistance, the interaction between the printing system and post-curing atmosphere was found and the printing system significantly affected the nano-wear resistance only in 2 subgroups post-cured without N_2 ($p < 0.001$). Meanwhile, for the soft material, 2-way ANOVA revealed that all the evaluated properties were significantly affected by both the printing system ($p = 0.001$ for the flexural modulus and $p < 0.001$ for all the others) and post-curing atmosphere ($p = 0.022$ for the flexural strength, $p = 0.005$ for the flexural modulus, $p = 0.006$ for the microhardness, $p = 0.004$ for the microwear resistance, $p < 0.005$ for all the others).

Table 1 shows the mean values and standard deviations of the flexural strength, flexural modulus, broken ratio, and microhardness. The data of flexural strength, flexural modulus, and microhardness in Creo-hard subgroups overlapped with those reported in the previous study (Wada et al., 2023). Generally, soft materials revealed significantly lower values than hard materials. Using the Asiga printer significantly enhanced the flexural strength only in soft materials post-cured without N_2 ($p = 0.002$), while the post-curing with N_2 revealed significantly lower flexural strength in hard materials additive-manufactured by the Creo printer ($p = 0.027$) and in soft materials additive-manufactured by the Asiga printer ($p = 0.023$). Meanwhile, using the Asiga printer revealed significantly higher flexural modulus only in soft materials post-cured without N_2 ($p = 0.025$), while the post-curing atmosphere revealed no significant effect both in hard and soft materials. For the broken ratio, both the printing system and post-curing atmosphere revealed no significant effect both in hard and soft materials. Using the Creo printer revealed significantly higher microhardness both in hard and soft materials regardless of the post-curing atmosphere ($p < 0.001$ for all), while the post-curing with N_2 revealed significantly higher microhardness in hard and soft materials additive-manufactured by the Asiga printer ($p < 0.001$ for all).

Fig. 3 shows the mean values and standard deviations of microwear depth as the representative value of microwear resistance. Soft materials generally revealed higher microwear resistance than hard materials. In hard materials, using the Asiga printer revealed significantly lower microwear depth only in the specimens post-cured with N_2 ($p = 0.014$), while the post-curing with N_2 revealed significantly lower values only in the specimens additive-manufactured by the Asiga printer ($p = 0.020$). In soft materials, using the Creo printer revealed significantly lower microwear depth in the specimens post-cured both without N_2 ($p = 0.021$) and with N_2 ($p < 0.001$), while the post-curing with N_2 revealed significantly lower microwear depth only in the specimens additive-manufactured by the Creo printer ($p = 0.007$).

Table 2 shows the mean values and standard deviations of reduced elastic modulus and nano surface hardness. Conventional materials including heat-cured and autopolymerizing resins generally revealed higher values both in the reduced elastic modulus and nano surface hardness than additive-manufactured hard materials. Both for hard and soft materials, significant differences both in two measures were revealed between each pair of 6 groups including conventional materials ($p < 0.001$ for all) except the reduced elastic modulus in the subgroup of soft materials additive-manufactured by the Asiga printer ($p = 0.231$). Creo groups revealed higher values in both measures than Asiga groups, while the post-curing with N_2 revealed lower values in both measures than that without N_2.

Fig. 4 shows the mean values and standard deviations of nano-wear depth as the representative value of nano-wear resistance. Hard materials generally revealed lower nano-wear depth than soft materials. Additionally, conventional materials revealed significantly lower nano-wear depth than additive-manufactured materials ($p < 0.001$ for all). Regardless of the printing system, the post-curing with N_2 significantly enhanced nano-wear resistance both in hard and soft materials ($p < 0.001$ for both Creo and Asiga hard subgroups, $p = 0.001$ for Creo soft subguroup, and $p < 0.001$ for Asiga soft subgroup). Regarding the printing system, using the Creo printer revealed significantly lower nano-wear depth in hard materials only when post-cured without N_2 than using the Asiga printer ($p < 0.001$), while using the Asiga printer revealed significantly lower nano-wear depth in soft materials than

Table 1
Mean values and standard deviations of flexural strength, flexural modulus, and microhardness, and results of 1-way ANOVA statistical analyses.

Material	Printing system	Post-curing atmosphere	Flexural strength (MPa)	Flexural modulus (Gpa)	Broken ratio (%)	Microhardness
AM hard			#	#	##	#
	Creo	- $	102.2 ± 1.9^{a}	2.60 ± 0.11^{a}	20	16.9 ± 0.2^{a}
		+ $	99.5 ± 3.4^{b}	2.54 ± 0.12^{a}	0	17.0 ± 0.2^{a}
	Asiga	–	$101.4 \pm 1.3^{a,b}$	2.61 ± 0.08^{a}	10	13.9 ± 0.5^{b}
		+	99.7 ± 0.7^{b}	2.59 ± 0.10^{a}	0	14.5 ± 0.4^{c}
AM soft			#	#	##	#
	Creo	–	33.3 ± 1.3^{A}	0.88 ± 0.05^{A}	0	7.1 ± 0.3^{A}
		+	33.2 ± 1.5^{A}	0.85 ± 0.07^{A}	0	7.1 ± 0.2^{A}
	Asiga	–	35.3 ± 0.8^{B}	0.94 ± 0.03^{B}	0	6.4 ± 0.8^{B}
		+	33.8 ± 0.5^{A}	$0.89 \pm 0.03^{A, B}$	0	5.8 ± 0.4^{C}

AM: additive-manufactured; -: stroboscopic post-curing in the air atmosphere; +: stroboscopic post-curing at a nitrogen gas atmosphere; #: same superscripted letters indicate groups not statistically significantly different when compared by Tukey multiple comparisons post hoc analysis; ##: Chi-squared test revealed no significant difference between materials post-cured without and with nitrogen gas, and $: Data reported in a previous study (Wada et al., 2023) were used for statistical analyses.

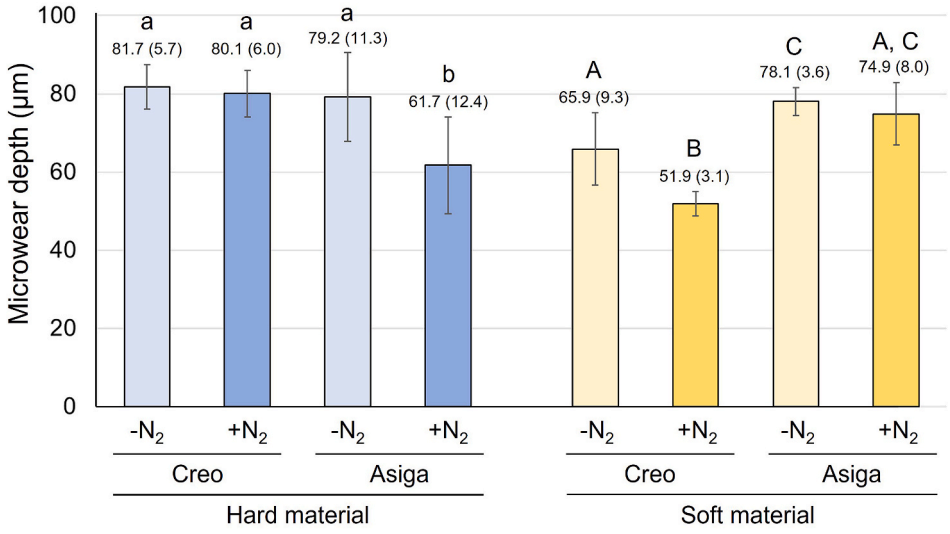

Fig. 3. Mean values (standard deviations) of microwear depth as microwear resistance. The same superscripted letters indicate groups not statistically significantly different when compared by 1-way ANOVA and post hoc analysis with Tukey multiple comparisons.

Table 2
Mean values and standard deviations of reduced elastic modulus and nano-hardness, and results of 1-way ANOVA statistical analyses.

Material	Printer type	Post-curing atmosphere	Reduced elastic modulus (GPa)	Nano surface hardness (MPa)
			#	#
AM hard	Creo	–	4.81 ± 0.09^{a}	251.9 ± 5.1^{a}
	Creo	+	4.60 ± 0.03^{b}	228.6 ± 4.2^{b}
	Asiga	–	4.10 ± 0.02^{c}	191.8 ± 2.9^{c}
	Asiga	+	3.59 ± 0.04^{d}	168.5 ± 3.7^{d}
Heat-cured	NA	NA	6.75 ± 0.04^{e}	332.8 ± 13.7^{e}
Autopolymerizing	NA	NA	6.25 ± 0.04^{f}	279.5 ± 9.5^{f}
			#	#
AM soft	Creo	–	4.86 ± 0.05^{A}	255.6 ± 4.4^{A}
		+	3.94 ± 0.03^{B}	184.5 ± 1.7^{B}
	Asiga	–	2.90 ± 0.03^{C}	128.0 ± 3.7^{C}
		+	2.58 ± 0.05^{C}	117.4 ± 2.3^{D}
Heat-cured	NA	NA	6.75 ± 0.04^{D}	332.8 ± 13.7^{E}
Autopolymerizing	NA	NA	6.25 ± 0.04^{E}	279.5 ± 9.5^{F}

AM: additive-manufactured; -: stroboscopic post-curing in the air atmosphere; +: stroboscopic post-curing at a nitrogen gas atmosphere; NA: not applicable, and #: same superscripted letters indicate groups not statistically significantly different when compared by Tukey multiple comparisons post hoc analysis.

using the Creo printer regardless of the post-curing atmosphere ($p = 0.003$ in specimens post-cured without N_2 and $p = 0.005$ in specimens post-cured with N_2).

Fig. 5 shows representative images for Creo group acquired by OP and AFM. Only the soft subgroups showed the bank-shaped prominence on the edge of wear facet in OP images, while both hard and soft subgroups showed the prominence in AFM images.

4. Discussion

This study demonstrated the effect of post-curing atmospheres on the micro- and nano-wear resistance of additive-manufactured materials for the hard and soft OSs. The overall results rejected the two null hypotheses and revealed that the 3D printing system and post-curing atmosphere as well as the material type affected the micro- and nano-wear resistance of the evaluated OS materials.

In this study, evaluated properties other than micro- and nano-wear depth of hard material generally showed higher values than those of soft materials (except reduced elastic modulus and nano surface hardness of Creo groups post-cured without N_2) (Tables 1 and 2). This was in agreement with the previous studies (Wada et al., 2022a, 2022b; Gibreel et al., 2021; Perea-Lowery et al., 2021). Nevertheless, regarding the microwear resistance, the wear depth of the hard material tended to be deeper than that of the soft material (Fig. 3). This finding suggested that hard material would not be necessarily more resistant to wearing stress than soft material. The elastic deformation of the soft material might

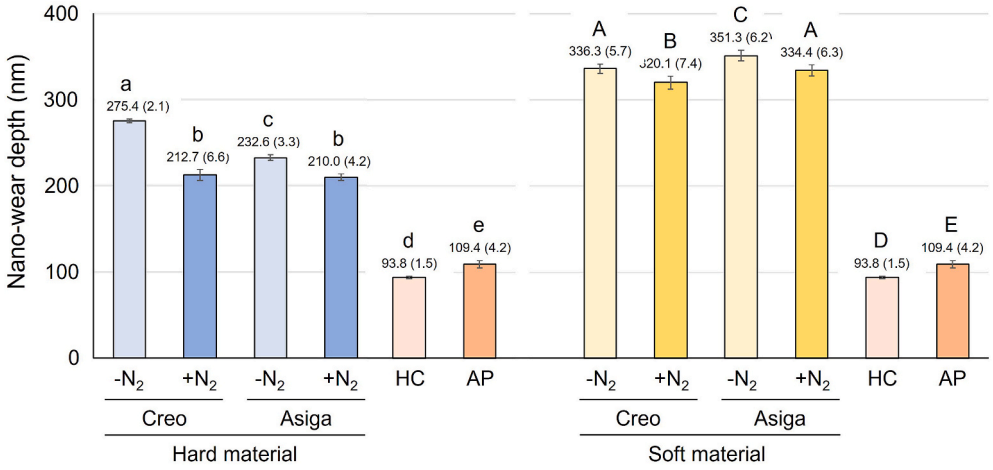

Fig. 4. Mean values (standard deviations) of nano-wear depth as nano-wear resistance. The same superscripted letters indicate groups not statistically significantly different when compared by 1-way ANOVA and post hoc analysis with Tukey multiple comparisons. HC: heat-cured resin, and AP: autopolymerizing resin.

provide some shock-absorbing ability that would lead to higher wear resistance in comparison with the hard material. In the OP images, the bank-shaped prominence (the plastic deformation) was confirmed only in the soft material (Fig. 5). Such a non-uniform deformation might prevent the deeper progression of wearing. On the other hand, the deformation can be a potential risk of wearing in disharmony with antagonists.

Nano-wear depths of soft materials were significantly deeper than those of hard materials (Fig. 4). In the AFM images after the nano-indentation wear test, the bank-shaped prominences were homogenously confirmed both in hard and soft materials and there was no optical difference in wear facets (Fig. 5). Nevertheless, a previous study reported that there was the optical difference in wear characteristic of thermoplastic denture base materials provided with nano-wear test (Hamanaka et al., 2016), indicating that the optical variety in wear facet image observed by AFM would depend on the tested materials.

The antagonist of the microwear testing device used in this study was a steatite ball, and tested specimens were rigidly fixed by the holder during microwear testing. Those structures of the microwear testing device would give the material-specific wear profiles (Fig. 5). Meanwhile, the antagonist of the nanoindentation device was a cube corner three-sided indenter with a face angle of 35.26° and tested specimens were magnetically fixed rigidly, allowing a small displacement of specimens when compared to microwear testing device. Those structures of the nanoindentation device would result in homogenous wearing profiles (Fig. 5). On the other hand, both in micro- and nano-wear tests, it was noted that the higher wear resistance was shown in subgroups additive-manufactured by DLP printer in the hard materials, while it was shown in subgroups additive-manufactured by LCD printer in the soft materials (Figs. 3 and 4). This finding indicated that recommended 3D printing system (DLP or LCD) would be dependent on the material type.

Strictly speaking, the Vickers hardness test and some other surface hardness measuring systems are not recommended to evaluate soft materials other than metals and ceramics due to their elastic recovery of the indentation mark. On the other hand, those tests for measuring surface hardness have been common for dental materials including soft materials, indicating that the data acquired by those tests could be indicative and scientifically discussed. In this study, VHN was measured 30 s after making the indentation and used as an indicative unit for surface hardness with special emphasis to standardize the influence of material shape recovery after indentation on the diameter of the indentation mark on the material surface.

Previous studies have reported that a stroboscopic post-curing at an N_2 atmosphere could prevent the oxygen-inhibited layer formation and enhance the degree of conversion on the surface layer of additive-manufactured objects, leading to the improvement of their physical properties (Shawkat et al., 2009; Reymus et al., 2019). Other studies have indicated that the effect of post-curing atmospheres would be limited only to the surface layer (Wada et al., 2022a, 2022b). In this study, during the polishing procedure, the surface layer of around 250 μm was removed from each specimen. Although a previous study reported that the effect of post-curing atmosphere would not be clearly confirmed in OS material additive-manufactured by an LCD printer (Wada et al., 2023), the current study revealed that using N_2 as a protection gas during post-curing enhanced the microwear resistance of Asiga hard subgroups and the nano-wear resistance of each subgroup (Figs. 3 and 4). This finding indicated that the effect of post-curing atmosphere would remain after the removal of surface layer with polishing. In addition to preventing the oxygen-inhibited layer formation, longer post-curing time (Aati et al., 2022) and higher post-curing temperature (Lim et al., 2022) can enhance the physical properties of additive-manufactured objects. In this study, the temperature of chamber and inside of the specimen during post-curing was 33 °C and 38 °C without N_2, while those were 36 °C and 42 °C with N_2. A previous study revealed that around 10 °C increase in the post-curing temperature would significantly enhance the physical properties of additive-manufactured objects (Tangpothitham et al., 2022). Although the difference in the post-curing temperature between without and with N_2 was rather small in this study, the post-curing temperature difference might affect the inner part of tested specimens.

The majority of previous studies have indicated that hard OSs would be more effective for treating TMD and/or protecting dentition from sleep bruxism (Okeson, 1987; Cruz-Reyes et al., 2011). Nevertheless, the stress that patients feel with wearing soft OSs would be milder than that with wearing hard OSs (Ariji et al., 2016). Additionally, it was reported that the brain activity in OS wearers would be higher when using hard materials than when using soft materials (Sriharsha, 2018), indicating that soft OSs would be more stressless for patients to wear than hard OSs. Regarding the additive-manufactured OS materials tested in this study, the soft material showed higher microwear resistance than the hard material when additive-manufactured using an LCD printer (Fig. 3). This finding agreed with the previous study in which the wear resistance of the soft material was comparable to the conventional hard OS material based on autopolymerizing polymethyl methacrylate (Gibreel et al., 2022). As mentioned before, the additive-manufactured soft OS material tested in this study showed plastic deformation in the wear facet, indicating its wear characteristics would not constantly keep harmony with the antagonist. However, the higher microwear resistance may combine comfortableness with practicality.

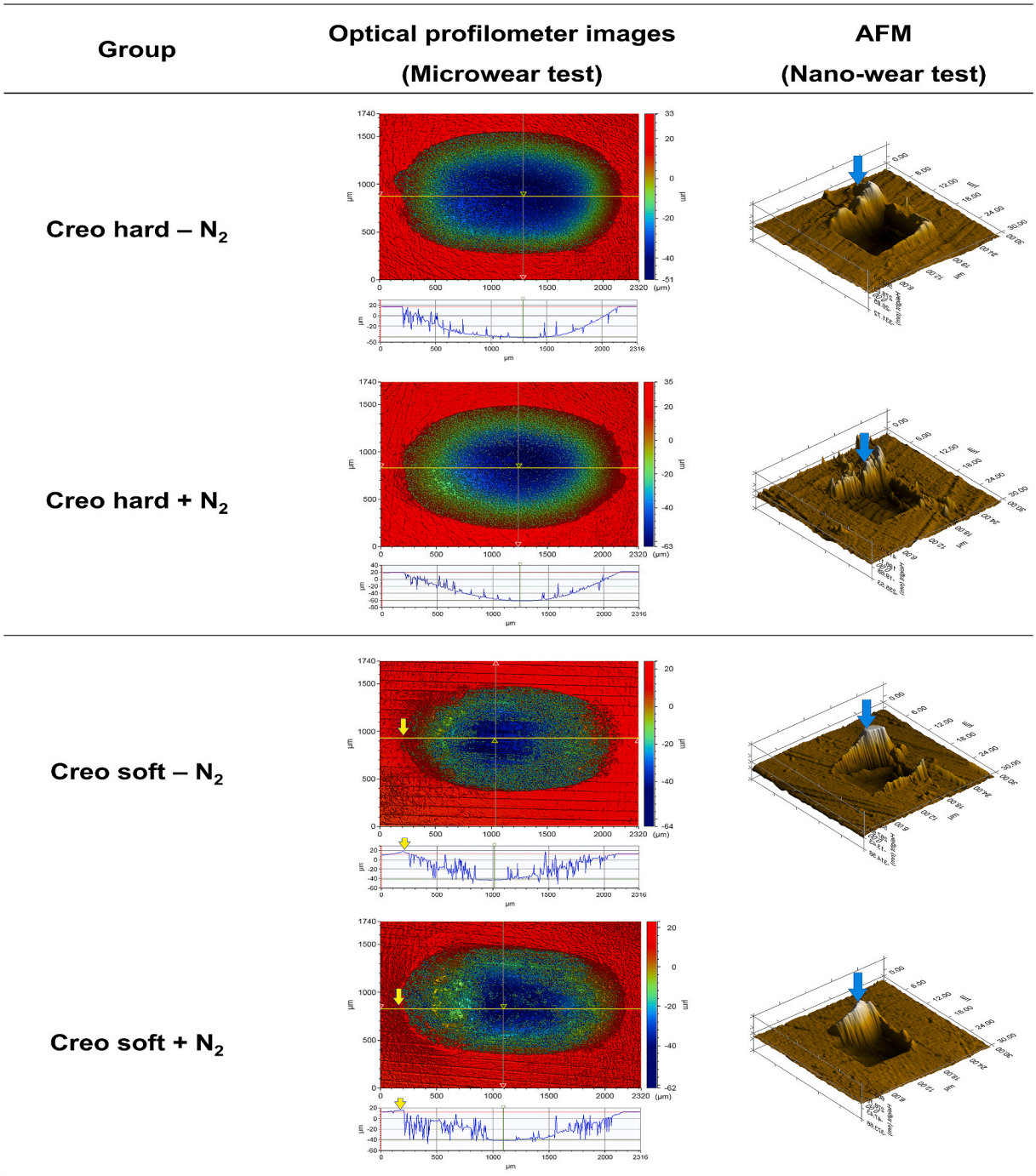

Fig. 5. Representative images of Creo groups acquired by optical profilometer (OP) after microwear test and those acquired by atomic force microscopy (AFM) after nano-wear test. X-axis profilometer scale shows profile on cross-sectional plane of yellow line on OP image. It was noted that only soft specimens showed bank-shaped prominence on facet edge (yellow arrow), while both hard and soft specimens showed those prominences (blue arrow).

There were several limitations in this study. First, the testing condition could not clinically simulate the appliance of OSs in the actual oral cavity. Ideally, further in vivo studies should be needed to evaluate the wear resistance under the clinical situation. Second, the post-curing time and temperature were not verified. Previous studies have reported that not only the atmosphere but also time and temperature during post-curing would affect the physical properties of additive-manufactured objects (Aati et al., 2022; Lim et al., J.H., 2022; Tangpothitham et al., 2022.), suggesting that further studies are necessary to clarify the effect of post-curing time and temperature on the wear resistance of OS materials. Third, the detailed composition data of tested materials for additive-manufactured occlusal splints was never clarified by the manufacturer. Therefore, it is still unclear whether any components of the tested materials would play a role in the results of this study or not. Future studies should be performed to evaluate the effect of surface polishing based on various material compositions. Finally, the printing layer thickness and orientation were unified in this study. Those factors would play a role in additive manufacturing (Perea-Lowery et al., 2021; Wulff et al., 2022). It should be investigated how the printing layer thickness and orientation would affect the wear resistance of additive-manufactured OSs in future studies.

5. Conclusion

Within the limitations of this study, the following can be concluded: (1) 3D printing system and post-curing atmosphere affect the micro- and nano-wear resistance of tested additive-manufactured OS materials; (2) the optimal printing system providing higher wear resistance depends on the material type, and (3) using nitrogen gas as a protection gas during post-curing enhances the wear resistance of tested OS materials.

Funding

This work was supported by the Japan Society for the Promotion of Science [grant number 20K10030].

CRediT authorship contribution statement

Junichiro Wada: Writing – review & editing, Writing – original draft, Visualization, Validation, Supervision, Software, Methodology, Investigation, Funding acquisition, Formal analysis, Data curation, Conceptualization. **Kanae Wada:** Writing – original draft, Methodology, Investigation, Data curation, Conceptualization. **Sufyan Garoushi:** Writing – review & editing, Methodology, Investigation, Formal analysis, Data curation. **Akikazu Shinya:** Validation. **Noriyuki Wakabayashi:** Validation. **Tsutomu Iwamoto:** Validation. **Pekka K. Vallittu:** Writing – review & editing, Supervision, Project administration, Conceptualization. **Lippo Lassila:** Writing – review & editing, Supervision, Software, Resources, Project administration, Methodology, Funding acquisition, Formal analysis, Conceptualization.

Declaration of competing interest

The authors declare the following financial interests/personal relationships which may be considered as potential competing interests: Junichiro Wada reports financial support was provided by Japan Society for the Promotion of Science. Lippo Lassila reports a relationship with Helsinki-Uusimaa Regional Council that includes: funding grants. Noriyuki Wakabayashi reports a relationship with Japan Society for the Promotion of Science that includes: funding grants. Tsutomu Iwamoto reports a relationship with Japan Society for the Promotion of Science that includes: funding grants. Kanae Wada reports a relationship with Japan Society for the Promotion of Science that includes: funding grants. Author Pekka K. Vallittu serves in an editorial capacity for the Journal of the Mechanical Behavior of Biomedical Materials as an associate editor.

Data availability

Data will be made available on request.

Acknowledgments

This study was carried out with the support of the Biocity Turku Biomaterials Research Program (www.biomaterials.utu.fi).

References

Aati, S., Akram, Z., Shrestha, B., Patel, J., Shih, B., Shearston, K., Ngo, H., Fawzy, A., 2022. Effect of post-curing light exposure time on the physico-mechanical properties and cytotoxicity of 3D-printed denture base material. Dent. Mater. 38, 57–67. https://doi.org/10.1016/j.dental.2021.10.011.

Al Hamad, K.Q., Al-Rashdan, B.A., Ayyad, J.Q., Al Omrani, L.M., Sharoh, A.M., Al Nimri, A.M., Al-Kaff, F.T., 2022. Additive manufacturing of dental ceramics: a systematic review and meta-analysis. J. Prosthodont. 31, e67–e86. https://doi.org/10.1111/jopr.13553.

Al-Moraissi, E.A., Farea, R., Qasem, K.A., Al-Wadeai, M.S., Al-Sabahi, M.E., Al-Iryani, G. M., 2020. Effectiveness of occlusal splint therapy in the management of temporomandibular disorders: network meta-analysis of randomized controlled trials. Int. J. Oral Maxillofac. Surg. 49, 1042–1056. https://doi.org/10.1016/j.ijom.2020.01.004.

Al Mortadi, N., Eggbeer, D., Lewis, J., Williams, R.J., 2012. CAD/CAM/AM applications in the manufacture of dental appliances. Am. J. Orthod. Dentofacial Orthop. 142, 727–733. https://doi.org/10.1016/j.ajodo.2012.04.023.

Anadioti, E., Kane, B., Zhang, Y., Bergler, M., Mante, F., Blatz, M.B., 2022. Accuracy of dental and industrial 3D printers. J. Prosthodont. 31, 30–37. https://doi.org/10.1111/jopr.13470.

Ariji, Y., Koyama, S., Sakuma, S., Nakayama, M., Ariji, E., 2016. Regional brain activity during jaw clenching with natural teeth and with occlusal splints: a preliminary functional MRI study. Cranio 34, 188–194. https://doi.org/10.1179/2151090315Y.0000000017.

Beier, U.S., Kapferer, I., Dumfahrt, H., 2012. Clinical long-term evaluation and failure characteristics of 1,335 all-ceramic restorations. Int. J. Prosthodont. (IJP) 25, 70–78. https://pubmed.ncbi.nlm.nih.gov/22259801/.

Cruz-Reyes, R.A., Martínez-Aragón, I., Guerrero-Arias, R.E., García-Zura, D.A., González-Sánchez, L.E., 2011. Influence of occlusal stabilization splints and soft occlusal splints on the electromyographic pattern, in basal state and at the end of six weeks treatment in patients with bruxism. Acta Odontol. Latinoam. 24, 66–74. https://europepmc.org/article/MED/22010409.

Ellakany, P., Fouda, S.M., Mahrous, A.A., AlGhamdi, M.A., Aly, N.M., 2022. Influence of CAD/CAM milling and 3D-printing fabrication methods on the mechanical properties of 3-unit interim fixed dental prosthesis after thermo-mechanical aging process. Polymers 14, 4103. https://doi.org/10.3390/polym14194103.

Faus-Matoses, V., Ruiz-Bell, E., Faus-Matoses, I., Özcan, M., Salvatore, S., Faus-Llácer, V. J., 2020. An 8-year prospective clinical investigation on the survival rate of feldspathic veneers: influence of occlusal splint in patients with bruxism. J. Dent. 99, 103352 https://doi.org/10.1016/j.jdent.2020.103352.

Garoushi, S., Lassila, L., Vallittu, P.K., 2021. Impact of fast high-intensity versus conventional light-curing protocol on selected properties of dental composites. Materials 14, 1381. https://doi.org/10.3390/ma14061381.

Gibreel, M., Perea-Lowery, L., Vallittu, P.K., Lassila, L., 2021. Characterization of occlusal splint materials: CAD-CAM versus conventional resins. J. Mech. Behav. Biomed. Mater. 124, 104813 https://doi.org/10.1016/j.jmbbm.2021.104813.

Gibreel, M., Perea-Lowery, L., Vallittu, P.K., Garoushi, S., Lassila, L., 2022. Two-body wear and surface hardness of occlusal splint materials. Dent. Mater. J. 41, 916–922. https://doi.org/10.4012/dmj.2022-100.

Goodacre, B.J., Goodacre, C.J., 2022. Additive manufacturing for complete denture fabrication: a narrative review. J. Prosthodont. 31, 47–51. https://doi.org/10.1111/jopr.13426.

Grymak, A., Waddell, J.N., Aarts, J.M., Ma, S., Choi, J.J.E., 2022. Evaluation of wear behaviour of various occlusal splint materials and manufacturing processes. J. Mech. Behav. Biomed. Mater. 126, 105053 https://doi.org/10.1016/j.jmbbm.2021.105053.

Halachmi, M., Gavish, A., Gazit, E., Winocur, E., Brosh, T., 2008. Splints and stress transmission to teeth: an in vitro experiment. J. Dent. 28, 475–480. https://doi.org/10.1016/s0300-5712(00)00026-9.

Hamanaka, I., Iwamoto, M., Lassila, L.V.J., Vallittu, P.K., Takahashi, Y., 2016. Wear resistance of injection-molded thermoplastic denture base resins. Acta Biomater. Odontol. Scand. 2, 31–37. https://doi.org/10.3109/23337931.2015.1135747.

Klasser, G.D., Greene, C.S., 2009. Oral appliances in the management of temporomandibular disorders. Oral Surg. Oral Med. Oral Pathol. Oral Radiol. Endod. 107, 212–223. https://doi.org/10.1016/j.tripleo.2008.10.007.

Kunjan, C., Jawahar, N., Chandrasekhar, U., 2006. Influence of layer thickness on mechanical properties in stereolithography. Rapid Prototyp. J. 12, 106–113. https://doi.org/10.1108/13552540610652456.

Kurt, H., Erdelt, K.J., Cilingir, A., Mumcu, E., Sülün, T., Tuncer, N., Gernet, W., Beuer, F., 2012. Two-body wear of occlusal splint materials. J. Oral Rehabil. 39, 584–590. https://doi.org/10.1111/j.1365-2842.2012.02301.x.

Li, X., Bhushan, B., 2002. A review of nanoindentation continuous stiffness measurement technique and its applications. Mater. Char. 48, 11–36. https://doi.org/10.1016/S1044-5803(02)00192-4.

Li, X., Wang, X., Bondokov, R., Morris, J., An, Y.H., Sudarshan, T.S., 2005. Micro/nanoscale mechanical and tribological characterization of SiC for orthopedic applications. J. Biomed. Mater. Res. B Appl. Biomater. 72, 353–361. https://doi.org/10.1002/jbm.b.30168.

Lim, J.H., Lee, S.Y., Gu, H., Jin, G., Kim, J.E., 2022. Evaluating oxygen shielding effect using glycerin or vacuum with varying temperature on 3D printed photopolymer in post-polymerization. J. Mech. Behav. Biomed. Mater. 130, 105170 https://doi.org/10.1016/j.jmbbm.2022.105170.

Lutz, A.M., Hampe, R., Roos, M., Lümkemann, N., Eichberger, M., Stawarczyk, B., 2019. Fracture resistance and 2-body wear of 3-dimensional-printed occlusal devices. J. Prosthet. Dent 121, 166–172. https://doi.org/10.1016/j.prosdent.2018.04.007.

McGuire, M.K., Nunn, M.E., 1996. Prognosis versus actual outcome. III. The effectiveness of clinical parameters in accurately predicting tooth survival. J. Periodontol. 67, 666–674. https://doi.org/10.1902/jop.1996.67.7.666.

Oja, J., Lassila, L., Vallittu, P.K., Garoushi, S., 2021. Effect of accelerated aging on some mechanical properties and wear of different commercial dental resin composites. Materials 14, 2769. https://doi.org/10.3390/ma14112769.

Okeson, J.P., 1987. The effects of hard and soft occlusal splints on nocturnal bruxism. J. Am. Dent. Assoc. 114, 788–791. https://doi.org/10.14219/jada.archive.1987.0165.

Oliver, W.C., Pharr, G.M., 2004. Measurement of hardness and elastic modulus by instrumented indentation: advances in understanding and refinements to methodology. J. Mater. Res. 19, 3–20. https://doi.org/10.1557/jmr.2004.19.1.3.

Perea-Lowery, L., Minja, I.K., Lassila, L., Ramakrishnaiah, R., Vallittu, P.K., 2021. Assessment of CAD-CAM polymers for digitally fabricated complete dentures. J. Prosthet. Dent 125, 175–181. https://doi.org/10.1016/j.prosdent.2019.12.008.

Quan, H., Zhang, T., Xu, H., Luo, S., Nie, J., Zhu, X., 2020. Photo-curing 3D printing technique and its challenges. Bioact. Mater. 5, 110–115. https://doi.org/10.1016/j.bioactmat.2019.12.003.

Revilla-León, M., Özcan, M., 2019. Additive manufacturing technologies used for processing polymers: current status and potential application in prosthetic dentistry. J. Prosthodont. 28, 146–158. https://doi.org/10.1111/jopr.12801.

Reymus, M., Lümkemann, N., Stawarczyk, B., 2019. 3D-printed material for temporary restorations: impact of print layer thickness and post-curing method on degree of conversion. Int. J. Comput. Dent. 22, 231–237. https://pubmed.ncbi.nlm.nih.gov/31463487/.

Shawkat, E.S., Shortall, A.C., Addison, O., Palin, W.M., 2009. Oxygen inhibition and incremental layer bond strengths of resin composites. Dent. Mater. 25, 1338–1346. https://doi.org/10.1016/j.dental.2009.06.003.

Sjöholm, T., Lehtinen, I.I., Helenius, H., 1995. Masseter muscle activity in diagnosed sleep bruxists compared with non-symptomatic controls. J. Sleep Res. 4, 48–55. https://doi.org/10.1111/j.1365-2869.1995.tb00150.x.

Sjoholm, T., Kauko, T., Kemppainen, P., Rauhala, E., 2014. Long-term use of occlusal appliance has impact on sleep structure. J. Oral Rehabil. 41, 795–800. https://doi.org/10.1111/joor.12201.

Sriharsha, P., Gujjari, A.K., Dhakshaini, M.R., Prashant, A., 2018. Comparative evaluation of salivary cortisol levels in bruxism patients before and after using soft occlusal splint: an in vivo study. Contemp. Clin. Dent. 9, 182–187. https://doi.org/10.4103/ccd.ccd_756_17.

Tangpothitham, S., Pongprueksa, P., Inokoshi, M., Mitrirattanakul, S., 2022. Effect of post-polymerization with autoclaving treatment on monomer elution and mechanical properties of 3D-printing acrylic resin for splint fabrication. J. Mech. Behav. Biomed. Mater. 126, 105015 https://doi.org/10.1016/j.jmbbm.2021.105015.

Tigmeanu, C.V., Ardelean, L.C., Rusu, L.C., Negrutiu, M.L., 2022. Additive manufactured polymers in dentistry, current state-of-the-art and future perspectives-A review. Polymers 14, 3658. https://doi.org/10.3390/polym14173658.

Tokiwa, O., Park, B.K., Takezawa, Y., Takahashi, Y., Sasaguri, K., Sato, S., 2008. Relationship of tooth grinding pattern during sleep bruxism and dental status. Cranio 26, 287–293. https://doi.org/10.1179/crn.2008.039.

Wada, J., Wada, K., Gibreel, M., Wakabayashi, N., Iwamoto, T., Vallittu, P.K., Lassila, L., 2022a. Effect of nitrogen gas post-curing and printer type on the mechanical properties of 3D-printed hard occlusal splint material. Polymers 14, 3971. https://doi.org/10.3390/polym14193971.

Wada, J., Wada, K., Gibreel, M., Wakabayashi, N., Iwamoto, T., Vallittu, P.K., Lassila, L., 2022b. Effect of 3D printer type and use of protection gas during post-curing on some physical properties of soft occlusal splint material. Polymers 14, 4618. https://doi.org/10.3390/polym14214618.

Wada, J., Wada, K., Gibreel, M., Wakabayashi, N., Iwamoto, T., Vallittu, P.K., Lassila, L., 2023. Effect of surface polishing on physical properties of an occlusal splint material for additive manufacturing under protection gas post-curing condition. Polymers 15, 625. https://www.mdpi.com/2073-4360/15/3/625.

Willems, G., Celis, J.P., Lambrechts, P., Braem, M., Vanherle, G., 1993. Hardness and Young's modulus determined by nanoindentation technique of filler particles of dental restorative materials compared with human enamel. J. Biomed. Mater. Res. 27, 747–755. https://doi.org/10.1002/jbm.820270607.

Wulff, J., Schweikl, H., Rosentritt, M., 2022. Cytotoxicity of printed resin-based splint materials. J. Dent. 120, 104097 https://doi.org/10.1016/j.jdent.2022.104097.